Direct Laser Pruning of CdS_xSe_{1-x} Nanobelts en Route to a Multicolored Pattern with Controlled Functionalities

Junpeng Lu,[†] Xiaodai Lim,[‡] Minrui Zheng,[†] Subodh G. Mhaisalkar,[§] and Chorng-Haur Sow[†,*]

[†]Department of Physics, National University of Singapore, 2 Science Drive 3, 117542, Singapore, [‡]Graduate School of Integrative Sciences and Engineering, National University of Singapore, 28 Medical Drive, 117456, Singapore, and [§]School of Materials Science and Engineering, Nanyang Technological University, Blk N4.1, Nanyang Avenue, 639798, Singapore

ABSTRACT CdS_xSe_{1-x} nanobelts are interesting nanostructured materials with a tunable band gap from 1.7 to 2.4 eV depending on the nanobelts' stoichiometry. On the basis of their chemical compositions, these nanobelts give out strong photoluminescence with unique color. In this work, we demonstrate that a direct focused laser beam irradiation was able to achieve localized modification of the chemical composition of the nanobelts. As a result, we could locally change the optical properties of these nanobelts. With a scanning laser beam, micropatterns with a wide range of fluorescence color could be created on a substrate covered with ternary nanobelts without a prepatterned mask. The laser modified nanobelts showed higher resistance to acid corrosion and these nanobelts exhibited more superior photoconductivity. The construction of micropatterns with functionality/color control within the sample would provide greater building blocks for photoelectronic applications.

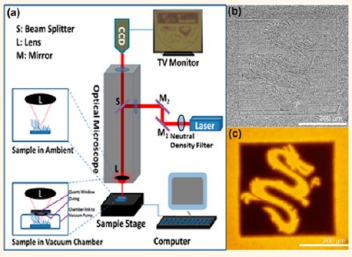

KEYWORDS: laser patterning · micropattern · nanoscale materials · optical and electrical property tuning

Band gap engineering is an attractive technique for the control of optical properties of semiconductors en route to potential applications. Utilizing the quantum confinement effect, altering the band gap by controlling the size dimension of materials is a common approach. In particular, this approach has been favored in the studies of one-dimensional (1D) semiconductor nanomaterials because of the ease in achieving confinement in the other two-dimensions for these nanomaterials. Owing to the rapid development of modern growth techniques, such as chemical vapor deposition, molecular beam epitaxy, and the hydrothermal approach, precise control of the size of 1D materials is now routinely achieved.[1] Through these methods, nanomaterials with unique optical and electrical properties can be synthesized.[2−5] However, for some applications, extreme reduction of the diameter of nanowires may not be desirable. For example, in nanolaser applications,[6−8] one may encounter the disappearance of the Fabry−Perot cavity for ultrathin nanowires, as a reasonably large dimension is required to avoid the diffraction limit. Thus, alternative approaches to modify and control the band gap of a semiconductor material are clearly desirable. For this purpose, band gap engineering by tuning the constituent composition of certain semiconductor alloys has been reported.[9,10] So far, 1D ternary alloyed semiconductors of CdS_xSe_{1-x},[11−13] ZnS_xSe_{1-x},[14,15] $Ag_2Se_{1-x}Te_x$,[16] $Zn_xCd_{1-x}S$/Se,[17−19] $Mn_xCd_{1-x}S$[20] and $Zn_{1-x}Mn_xSe$[21] nanowires or nanoribbons have been synthesized through template-assisted electrodeposition or chemical vapor deposition methods. These materials are exploited in the fabrication of field effect transistors, solar cells, and laser diodes but their extensive applications are constrained by the typical heterogeneous composition of these materials.[9,12] More recently, we reported a simple but efficient one-step method to synthesize ternary CdS_xSe_{1-x} nanobelts with uniform and controllable composition.[22] Once samples with uniform composition are fabricated, in light of interest to miniaturize a functional device, it is worthwhile to develop techniques which can further create micropatterns with controlled functionalities on these samples. These techniques should be able to directly pattern the nanomaterials as well as alter the optical properties of the ternary alloys during the process. Therefore, a simple, flexible, efficient, and low cost multipurpose postprocessing technique is highly desirable. So far, several innovative patterning methods have already been reported. These include nanoimprinting,[23,24] microcontact

* Address correspondence to physowch@nus.edu.sg.

Received for review July 5, 2012 and accepted August 27, 2012.

Published online August 27, 2012
10.1021/nn303000j

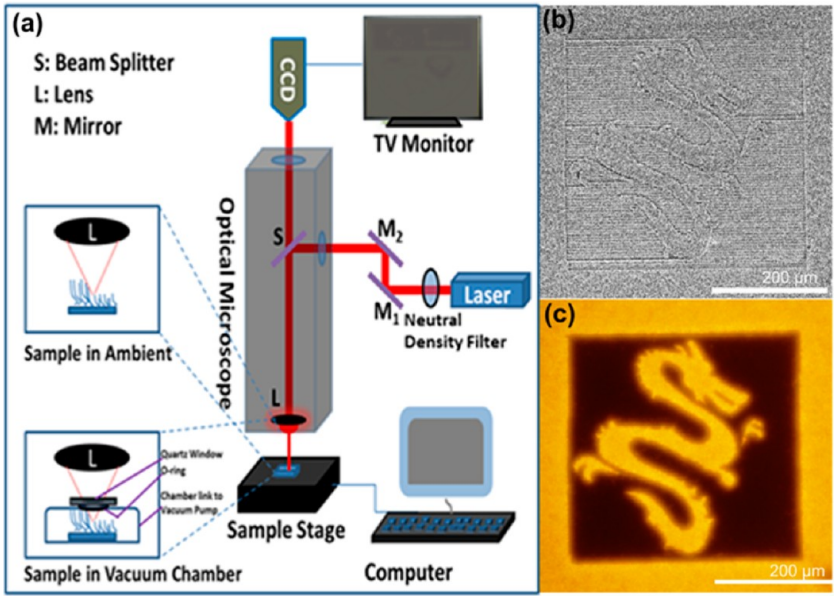

Figure 1. (a) Schematic of the optical microscope-focused laser beam setup for micropatterning. (b) SEM and (c) fluorescence microscopy images of a "dragon" patterned *via* a 660 nm laser with a power of 30 mW.

printing,[25] soft lithography,[26] dip-pen lithography,[27] photolithography,[28] and inkjet printing.[29] Each of these techniques has specific advantages and drawbacks. For example, most of the methods involved employment of masks to define the patterns with postprocessing treatment for the removal of photoresist. These processes often destroy or compromise the optical properties of the delicate nanomaterials. In this work, we present a facile and effective focused laser pruning method that can controllably modify the chemical composition of the nanobelts. In doing so, we can control the photoluminescence properties of the nanobelts. This is a surprising result considering the more conventional destructive nature of the focused laser beam. With a scanning focused laser beam, multicolored micropatterns can be fabricated on an extended area on a substrate covered with the nanobelts. Moreover, the fabrication of the micropatterns does not require the use of any predefined mask. Hence this method reduces the risks of physical damage and chemical contamination to the sample. The possible chemical modifications were systematically investigated by photoluminescence spectroscopy, energy-dispersive spectroscopy, X-ray photoelectron spectroscopy, and X-ray diffractometry. To the best of our knowledge, this is the first report on the modification of the chemical composition of the ternary CdS_xSe_{1-x} compound utilizing a focused laser technique.

RESULTS AND DISCUSSION

CdS_xSe_{1-x} nanobelts with highly uniform stoichiometry were synthesized through a facile one-step VLS process, as reported previously.[22] With this approach, ternary alloyed CdS_xSe_{1-x} nanobelts with uniform composition covering a large homogeneous area on a substrate (1 cm × 1 cm) were easily obtained. Both optical pictures and SEM images of as grown samples with uniform stoichiometry are shown in the Supporting Information (Figure S1).

After the successful synthesis of the ternary alloyed CdS_xSe_{1-x} nanobelts with high uniform composition, we subjected the alloy to a treatment of focused laser beam destruction with the aim to create micropatterns on the substrate. However, instead of destroying the nanobelts, we found that the focused laser beam could effectively modify the chemical nature of the nanobelts and more importantly change the photoluminescence nature of the nanobelts. With this feasibility, we could carry out localized bandgap engineering on a sample and create different components on the same sample.

The direct micropatterning and micromodification was carried out through an optical microscope-focused laser beam setup. Figure 1a shows a schematic diagram of our experimental setup. In this setup, a diode laser (maximum power = 60 mW, λ = 660 nm) was employed. The emitted parallel laser beam was introduced into an optical microscope *via* two mirrors. The power of the laser beam was adjusted by a neutral density filter inserted along the optical train. Inside the microscope, the laser beam was directed toward the objective lens (*L*, magnification = 50×) by a beam splitter (S). The laser beam was tightly focused onto the surface of a sample *via* an objective lens. The sample was mounted on an *X*−*Y* stage (motorized stage MICOS) which was controlled by a computer. A CCD camera was used to capture the optical images. Hence we could monitor the process of laser pruning and examine the quality of the pattern directly. Apart from micropatterning with the sample in ambient condition, a vacuum chamber (2 cm × 1 cm × 0.5 cm)

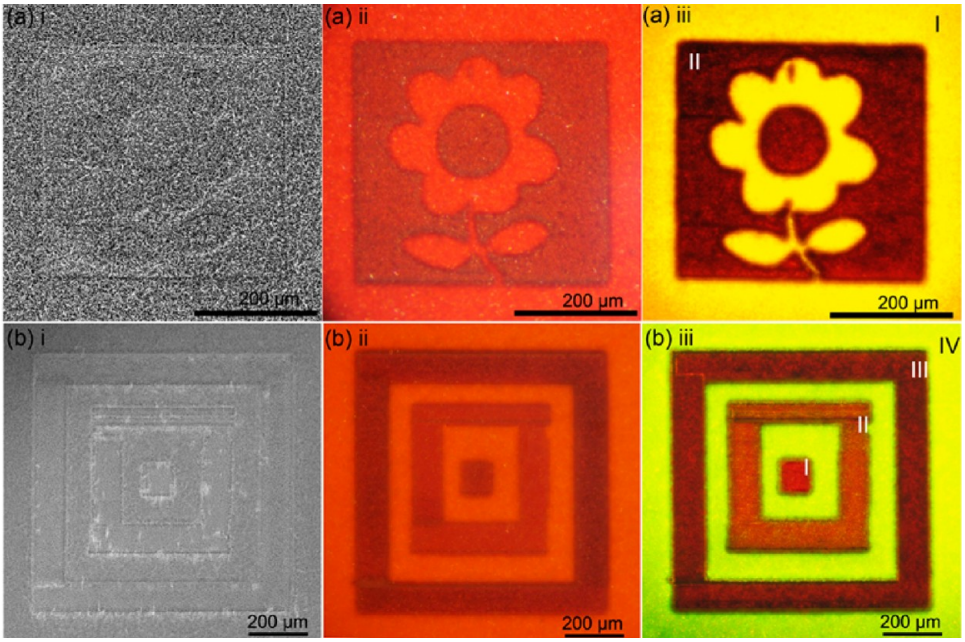

Figure 2. (a) (i) SEM, (ii) optical microscope, and (iii) fluorescence microscope images of a "flower" patterned on $CdS_{0.75}Se_{0.25}$ nanobelts film *via* a focused laser beam (wavelength: 660 nm) at a power of 20 mW. (b) (i) SEM, (ii) optical microscope, and (iii) fluorescence microscope images of boxes patterned on $CdS_{0.79}Se_{0.21}$ nanobelts film: multicolored pattern with four different colors obtained by careful control of the laser power.

could be used to house the sample. The laser could be focused toward the sample through a quartz window positioned on the top of the chamber. A vacuum pump was linked to the chamber, and thus the sample could be modified in vacuum condition. In addition, we could also fill the chamber with helium gas to control the gaseous environment during the laser irradiation.

When the laser beam was focused upon a film of nanobelts, the absorbed laser energy was rapidly converted to local heat. The intense heat raised the temperature of irradiated nanobelts and caused localized partial modification of the ternary alloys. This method is akin to plant pruning and thus it is denoted as the laser pruning method. By controlling the sample stage movement in a programmable manner with respect to the focused laser beam, micropatterns were constructed on the nanobelts covered surface. Figure 1b shows an SEM image of a pattern created using this laser pruning method and Figure 1c shows the same pattern as observed using a fluorescence microscope (FM). The bright orange background is reminiscent of the optical properties of the $CdS_{0.71}Se_{0.29}$ nanobelts. Remarkably, the laser modified region was also optically active and exhibited a different fluorescent color. The "dragon" was created *via* a laser power of 30 mW. Figure 2 provides further illustrations on the appearance of the patterned samples when they were imaged by SEM, optical microscope, and FM, respectively. The SEM image (Figure 2a,i) did not reveal a striking contrast from the complex microstructure created. This was attributed to the relatively low laser power (20 mW) used, and hence the morphology of the $CdS_{0.75}Se_{0.25}$ nanobelts was not significantly affected. However, the reflectivity of the laser pruned areas became different from the pristine areas. As a result, the optical image provided a clearer distinction and the micropattern became more visible (Figure 2a,ii). Perhaps the most dramatic change in the nanobelts was revealed by the image captured using the fluorescence microscope (Figure 2a,iii). CdS_xSe_{1-x} nanobelts have been demonstrated to possess high yield luminescence.[12,22] Therefore, intense light emission was achievable upon UV excitation. Remarkably, laser treated nanobelts had a different fluorescent color and the difference in this color from the pristine nanobelts resulted in the best contrast among the three types of images. Clearly, the laser treated nanobelts had transformed into a different type of material with different fluorescence property. This is a surprising finding considering the destructive attribute of a focused laser beam. The color can be readily regulated and further altered by carefully controlling the power intensity of the laser beam. Figure 2b shows another example of a multicolored pattern with four different colors (as labeled in Figure 2b,iii). These boxes were formed on a $CdS_{0.79}Se_{0.21}$ sample created *via* laser pruning at different laser powers. Note that the difference in color between the pristine samples shown in panels a,iii and b,iii is due to the difference in the stoichiometry of the sample (see Supporting Information).

Systematic studies on the dependence of such laser modification on the power of the laser beam were carried out. Figure 3a shows a set of patterned microsquares (200 μm $\times$ 200 μm) created on $CdS_{0.71}Se_{0.29}$ nanobelts using laser beam with different laser power.

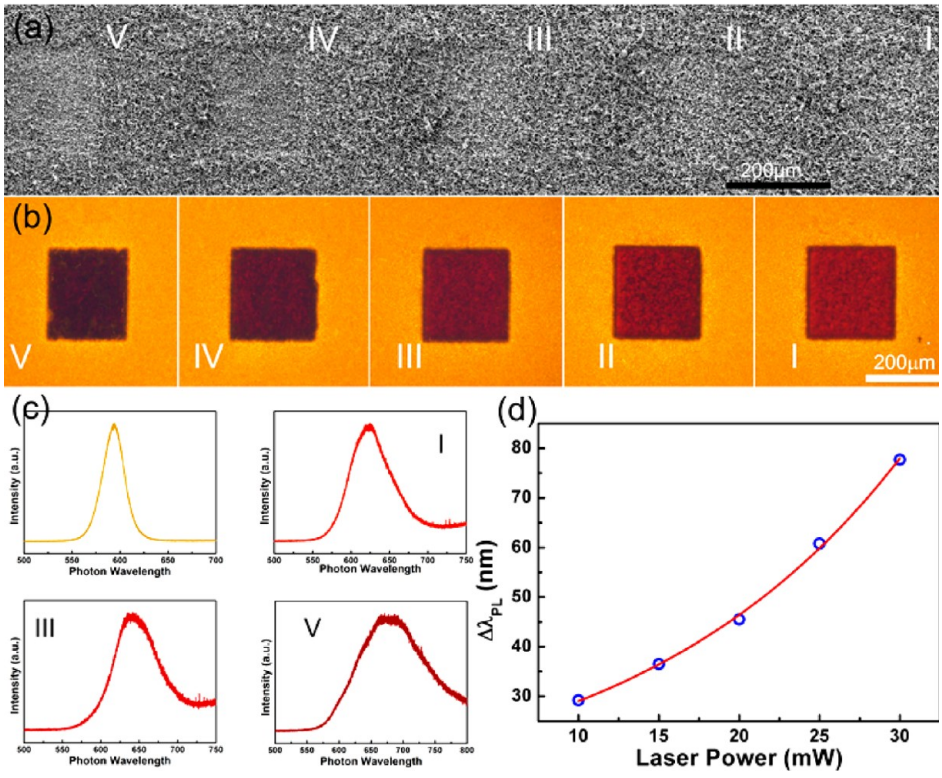

Figure 3. (a) SEM images of five microsquares patterned on $CdS_{0.71}Se_{0.29}$ nanobelts *via* different laser powers. [V (30 mW), IV (25 mW), III (20 mW), II (15 mW), and I (10 mW)]. (b) Corresponding fluorescence images of the five microsquares. (c) PL spectra of as-grown region and three representative patterned microsquares. (d) PL peak position shifts as a function of laser power.

The laser power was increased from 10 to 30 mW in the steps of 5 mW corresponding to patterns from I to V (right to left in the figure). Evidently, from I to V, the microsquares gradually deepened, attributable to the increasing laser power. It is interesting to note that pattern I was barely observable from the SEM image. To investigate the variation of color emission, FM images of these squares were captured and shown in Figure 3b. With increasing laser power, a darker red color was seen emitting from the pruned region. By altering the power from 10 to 30 mW, the corresponding patterns showed color covering a decent range from bright red to dark red.

Photoluminescence (PL) spectra for each of these regions were captured as well. As shown in Figure 3c, the pristine region and patterns I to V exhibited distinct PL peaks at different wavelengths. The pristine region showed a narrow and symmetrical peak located at 593.9 $\pm$ 0.1 nm. This corresponded to the orange color from the FM observation. After patterning with a low power of 10 mW, the PL peak of region I red-shifted by a large step from 593.9 $\pm$ 0.1 nm to 623.1 $\pm$ 0.1 nm. Visually, the emitted color changed from orange to bright red (region I). With increasing laser power in the steps of 5 mW until 30 mW, the corresponding PL peaks of regions II, III, IV, and V were identified at 630.4 $\pm$ 0.1 nm, 639.4 $\pm$ 0.1 nm, 654.7 $\pm$ 0.1 nm, and 671.6 $\pm$ 0.1 nm, respectively. Notably, the PL spectra of the pruned regions had become broadened and asymmetrical. The broadening of the peak is attributed to the increase in surface states or defect states resulting from laser ablation.[30,31] With the increase in laser power, the darkened color could further enhance the contrast between pruned and pristine regions and in turn facilitate a better image contrast of the micropatterns. The color modification is quantitatively described by Figure 3d, in which the shift in PL peak position, $\Delta\lambda$, from the PL peak position of the pristine $CdS_{0.71}Se_{0.29}$ nanobelts is plotted as a function of laser power. The experimental data (blue circles) can be fitted very well by a quadratic function, indicating the monotonically increasing relationship between red shifting in PL peak *versus* laser power.

Besides the shift in emission color, the morphology modification also exhibited a direct dependence on laser power. The striking morphological effects caused by laser pruning of nanobelts in ambience were observed through SEM. We exposed a CdS_xSe_{1-x} sample with x value of 0.68 to the focused laser beam. The SEM image shown in Figure 4a reveals the channels cut with a strong laser power of about 60 mW. The magnified view shown in the inset clearly illustrates two distinct and well-defined channels with a width of $\sim$1 μm separated by $\sim$10 μm. A clear separation between the pruned and pristine nanobelts was obtained. The result indicated that high spatial resolution is achievable with this direct pruning technique. A cross sectional image of a line channel is shown in Figure 4b.

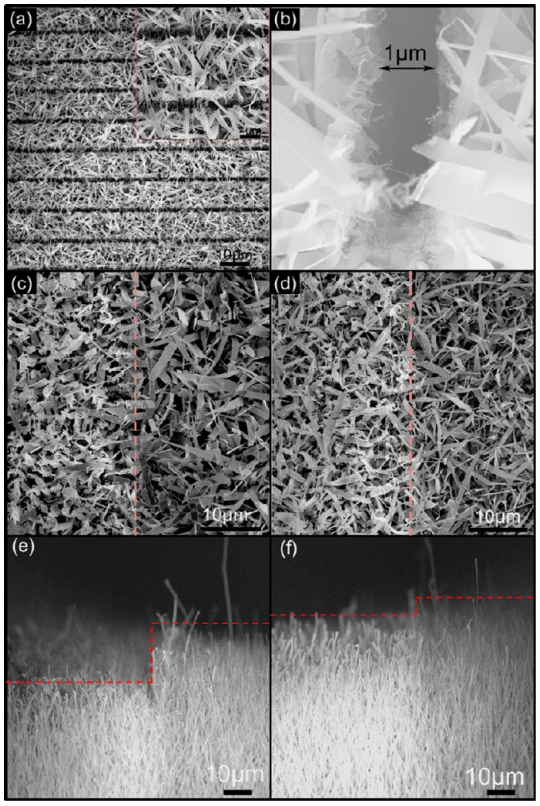

Figure 4. (a) SEM image of an array of microchannels. Magnified view in inset shows two distinct 1 μm channels separated by a width of 10 μm. (b) A cross sectional SEM image of a channel reveals the high spatial resolution of the focused laser beam technique. (c and d) Magnified images of the boundary of laser modified region (left) with pristine region (right). The powers of the laser used were 30 mW and 10 mW, respectively. (e and f) Cross sectional SEM views of the samples shown in images c and d, respectively.

The magnified views of laser treated sample clearly illustrate the physical distinctions of the morphology caused by different laser powers. As shown in Figure 4c, after exposure to a focused laser beam at 30 mW, the film of CdS_xSe_{1-x} nanobelts showed a distinct boundary (red dashed line) between the pruned and pristine areas. As revealed by the side-view SEM image (Figure 4e), the length of the film was obviously shortened by about 20 μm. And clearly the laser pruned surface became populated with blistered nanobelts, a clear contrast from the pristine nanobelts with smooth edges. On the other hand, for the square exposed to a focused laser beam at 10 mW (Figure 4d), the boundary was less noticeable. The length of the nanobelts became only slightly shortened (Figure 4f). Similarly, the morphology of the nanobelts changed from those with smooth edges to blistered form.

The color modification and morphology changes could be initially ascribed to a laser-induced thermal effect from the laser power dependence. Further characterizations are shown in Figure 5. As is well-known, the band gap energy for CdS and CdSe is 2.44 and 1.73 eV, respectively. These band gaps correspond to PL emission wavelength of 507 and 713 nm, respectively. Consequently, the significant red-shift observed from the PL spectra is attributed to the "S" element being driven away from the CdS_xSe_{1-x} nanobelts and the near-band-edge energy shift toward to CdSe. Briefly, the focused laser beam resulted in a high local temperature, which might dissociate the Cd═S bond and thus increase the relative concentration of CdSe species. To expound this proposed mechanism, we carried out energy-dispersive spectroscopy (EDS) analysis on a pristine region and region pruned with a laser power of 20 mW. As shown in Figure 5a, the ratio of "S/Cd" was measured to be 0.69 for the pristine region. On the other hand, the same ratio for the pruned region was significantly reduced to 0.49 as shown in Figure 5b. At the same time, the component of "Se" did not show any significant change after the laser pruning. In addition, "O" element was detected in the pruned region, which indicates the formation of an oxide phase. The broadness and asymmetry of the PL spectra after pruning (Figure 3c) could be attributed to defect contributions from the oxidation.

To further investigate the chemical process during the pruning process, X-ray photoelectron spectroscopy (XPS) was carried out for pristine and pruned regions. The XPS spectra are shown in Figure 5c,d. The S 2p peaks at 164.1 and 165.3 eV show a significant decrease after laser pruning. (the peaks were fitted and separated by 100% Gaussian profile). XRD studies were carried out before and after laser pruning as well. The results are shown in Figure 5 panels e and f, respectively. Evidently, there was a small left-shift, which reveals the modification of chemical composition,[22] of the CdS_xSe_{1-x} pattern after pruning. In addition, three prominent emerging peaks are observed at 33° ± 0.1°, 38.3° ± 0.1°, and 55° ± 0.1°, which are consistent with the (111), (200), and (220) peaks of CdO, respectively, as referenced to JCPDS No. 75-0594.

The formation of the oxide indicates that oxygen plays an important role in chemical modification process induced by the focused laser beam. To further explore the role of oxygen, a specially designed vacuum chamber, as shown in Figure 1, was employed to prune the ternary nanobelt in vacuum or in a chamber filled with helium gas to exclude the impact of oxygen. Surprisingly, the photoluminescence spectrum reveals a completely different appearance. As shown in Figure 6a, the red curve indicates the PL spectrum of the pruned region created in helium environment. The near-band-edge peak position after laser modification does not show any significant shift but a large and broad defect peak located in the infrared region is displayed. The emerging broad peak is attributed to the introduction of defects caused by the destruction of the good crystalline lattice due to the laser pruning. However, in

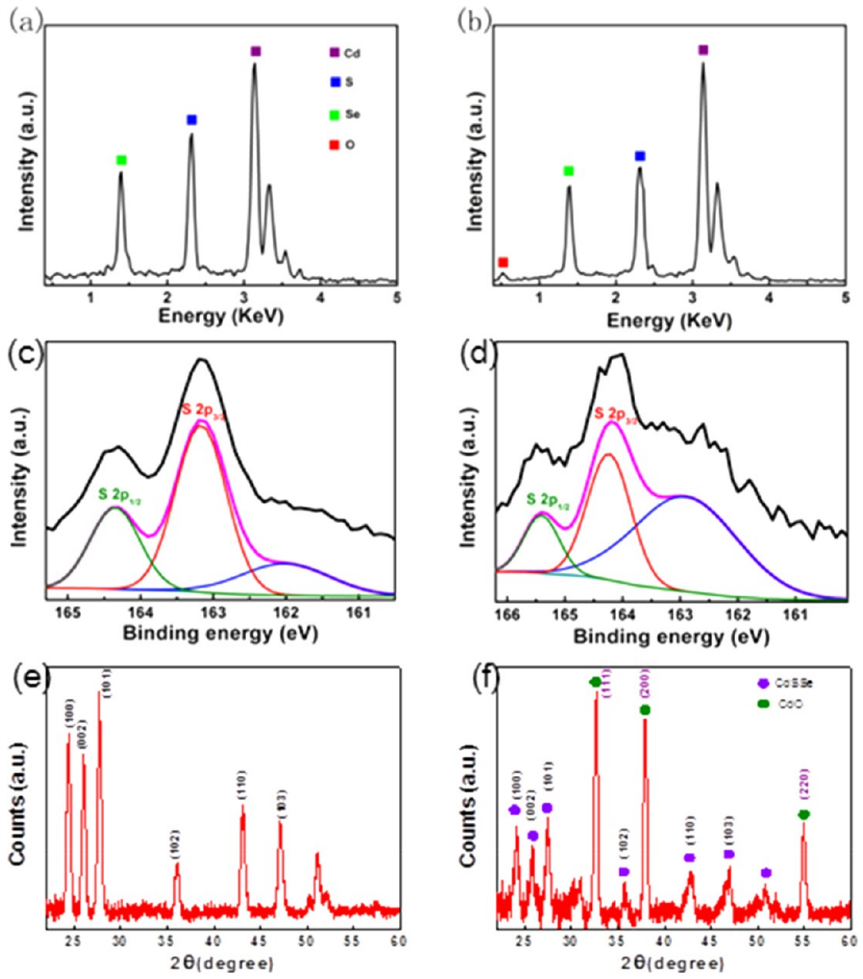

Figure 5. EDS spectra of $CdS_{0.69}Se_{0.31}$ nanobelts (a) before and (b) after laser modification. XPS spectra of these nanobelts (c) before and (d) after laser modification. XRD patterns of $CdS_{0.69}Se_{0.31}$ nanobelts (e) before and (f) after laser modification.

the absence of oxygen, the laser induced chemical modification of the $CdS_{0.75}Se_{0.25}$ nanobelts could not take place, hence there is no peak shift.

As further verification of the importance of heating with the presence of oxygen, we carried out additional experiments where the samples were annealed in ambient conditions. In three separate experiments, three pieces of $CdS_{0.75}Se_{0.25}$ nanobelts film (5 mm × 5 mm) were inserted into a horizontal tube furnace and then annealed in ambient condition at 650, 850, and 1050 °C, respectively. The duration of the heating was 0.5 min. The fluorescence images and corresponding PL spectra of the samples before and after annealing are shown in Figure 6b. Clearly, the fluorescence images showed a transition from orange color to light red and then dark red color. The PL peak position was found to be red-shifted and became broader and asymmetrical. All these are of course very similar to the fluorescence image and PL spectra obtained with laser pruning (Figure 3). In addition, the resultant XRD patterns (Supporting Information Figure S3) are almost identical to the XRD patterns obtained from laser pruned sample. Therefore, the proposed mechanism of laser-induced heating with oxidation as the main driving force for local chemical modification of the CdSSe nanobelts is tenable. As a further study, the local temperature under laser illumination was simulated by the finite element method (FEM) and the results showed that the laser heated spot on the sample could attain a temperature that is more than 800 °C. Details of the simulation are presented in Supporting Information Figure S2.

On top of the fabrication of a multicolored display, we found that the modified nanobelts are more stable when they were exposed to mild acid. Figure 7a illustrates a simple experiment that was carried out to explore the stability of pristine nanobelts and laser treated nanobelts toward exposure to acid (HCl). First we took a sample with $CdS_{0.73}Se_{0.27}$ nanobelts and created a "Tai Chi" micropattern. The fluorescence microscope image of the micropattern is shown in Figure 7d. The sample with the micropattern was fixed on top of a glass beaker with 5 mL of diluted HCl with a concentration of about 10%. After a short exposure (5 s) to the HCl vapor, the sample was collected and imaged by fluorescence microscope again. The corresponding

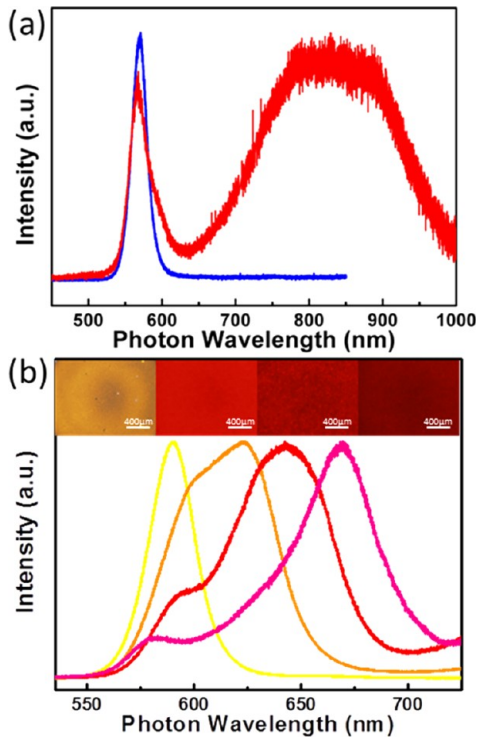

Figure 6. (a) PL spectra of pristine sample $CdS_{0.75}Se_{0.25}$ (blue curve) and sample after laser pruned in helium environment (red curve). (b) PL spectra of an as-grown $CdS_{0.75}Se_{0.25}$ sample (yellow curve) and three other samples after annealing with increasing temperatures of 650, 850, and 1050 °C for 0.5 min. Insets show the corresponding images of the samples captured by a fluorescence microscope.

FM image after exposure to HCl is presented in Figure 7e. Notably, the contrast of the FM image improved significantly after acid exposure. Figure 7 panels b and c display the PL spectra of pristine and pruned regions before and after acid exposure, respectively. Clearly, the PL emission peaks of both the laser pruned and pristine regions did not show any peak shift. Instead, the dominant change for the spectra is that the output intensity of pristine region shows an obvious decrease after acid treatment. Evidently pristine nanobelts are much more susceptible to acid corrosion. As for the laser pruned region, the laser heating introduced defective and oxidized states on the nanobelt, providing a more stable state against acid corrosion. With both pristine and laser pruned regions fluorescing at comparable intensity, the contrast of the image naturally became better. Such an attribute could be further exploited to develop the patterned nanobelts as potential acid sensors.

Besides the alteration in the optical properties, changes in the functionalities of the laser pruned nanobelts were also found in their electrical and photoelectrical properties. Figure 8a shows the typical $I-V$ curves for pristine nanobelts and laser pruned nanobelts. Clearly, the pristine nanobelts are poor conductors. We detected only a small current of $\sim 2.7 \times 10^{-10}$ A through the sample at an applied voltage of 5.0 V. However, after laser pruning, the sample showed a significant increase in conductivity. We measured a current of 1.3×10^{-8} A at an applied voltage of 5.0 V. Such an improvement can be attributed to the laser induced nanobelts modifications and also the improved nanobelts-to-nanobelts contact. These results shed light on the potential for a simple one-step, maskless, and *in situ* lithographic method for creating selective conducting domain. Besides a clear difference in conductivity, the pristine nanobelts and laser pruned nanobelts also exhibited marked difference in photocurrent. Figure 8 panels b and c show the typical $I-V$ curves of CdS_xSe_{1-x} nanobelts before and after laser pruning under broad beam laser illumination (1mW, $\lambda = 660$ nm). Both samples exhibited increased output current under illumination, indicating their obvious photoresponse to 660 nm laser light. However, the laser pruned sample shows a higher photoresponsivity than pristine nanobelts. Figure 8f presents the on/off photocurrent response corresponding to the laser illumination at 5 V bias under ambient condition. A rapid and prominent photoresponse was observed for both samples with the on/off laser illumination. The photocurrent of pristine nanobelts increased 5 times compared to that measured at dark condition. However, under the same illumination condition, the laser pruned sample exhibited 10 times increase in current, as shown in Figure 8f (green curve). Besides the response to visible spectrum light, the laser pruned nanobelts also exhibited sensitive response to infrared light. Figure 8 panels d and e display typical $I-V$ curves of pristine and pruned nanobelts under 1 mW 808 nm laser illumination. Evidently, the pristine sample did not show any change in the output current while the output current of pruned nanobelts increased dramatically. As shown in Figure 8g, the pruned sample (brown curve) exhibited a rapid and prominent on/off photoresponse to 808 nm laser at 5 V bias, while the current passing through the pristine sample remained constant under the same irradiation and bias condition. In Supporting Information Figure S4, we show that a pristine sample after being annealed in 650 °C also exhibited photoresponse to 808 nm laser but the output photocurrent was lower. The higher photoresponsivity of the pruned nanobelts could be attributed to the change of the optical property after laser pruning. The red-shift in the PL and the reflection spectrum (Figure S5) of the nanobelts was suggestive of a material that exhibited better photoresponse near to the wavelength of illumination (660 nm and 808 nm). These findings demonstrated the enhanced photoelectrical properties of laser pruned CdS_xSe_{1-x} nanobelts and indicated their potential in optoelectronic applications such as photoswitching and wavelength selective photosensors.

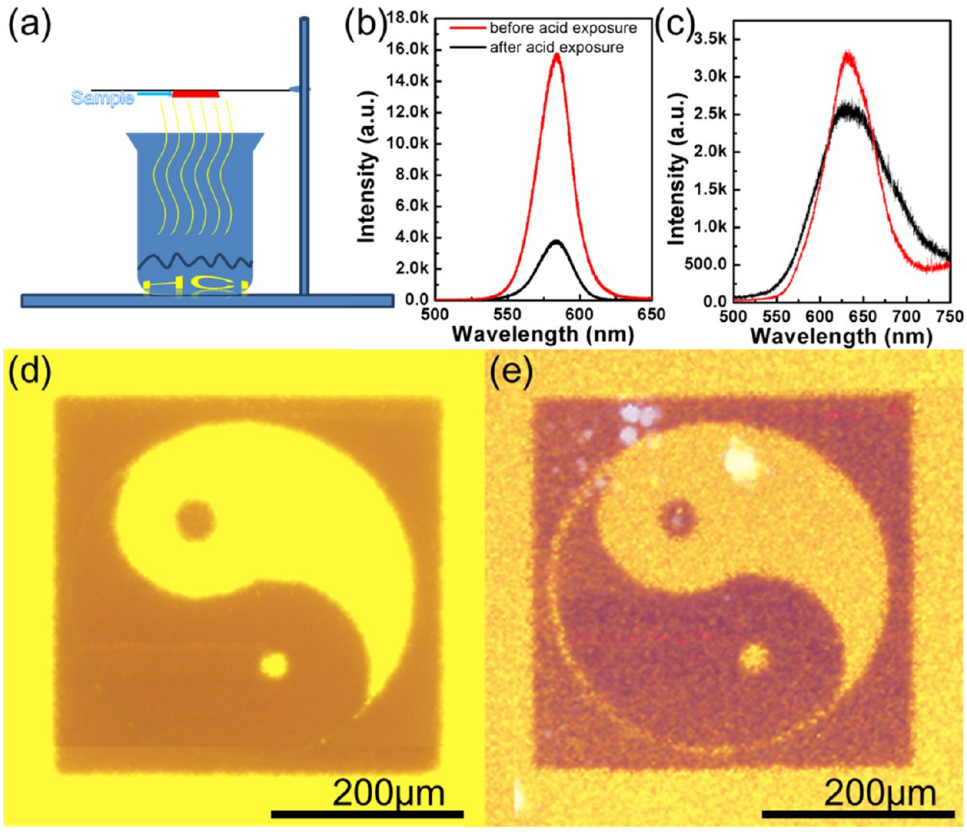

Figure 7. (a) Schematic of the setup for the studies on acid-exposure . PL spectra of (b) pristine and (c) pruned region before and after acid exposure. Fluorescence microscope images of a micro-Tai Chi pattern (d) before and (e) after acid exposure.

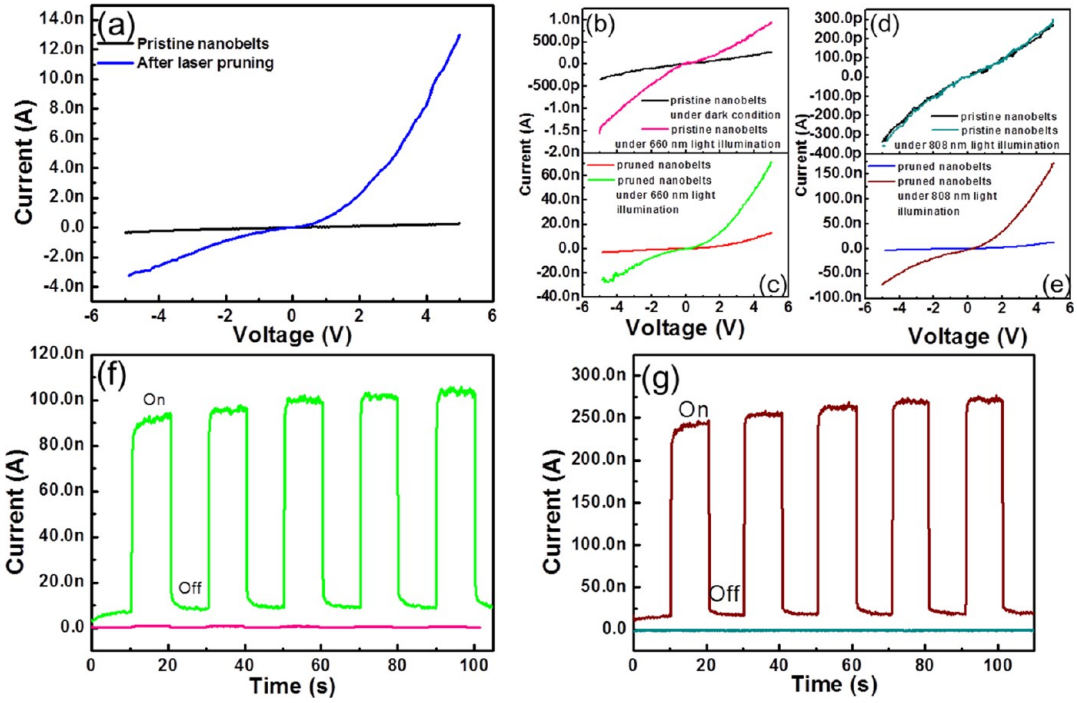

Figure 8. (a) Typical *I*–*V* curves acquired with two-probe measurements for the pristine nanobelts film and its laser pruned counterpart. Typical *I*–*V* curves under 660 nm laser irradiation of (b) pristine and (c) pruned nanobelts film. Typical *I*–*V* curves under 808 nm laser irradiation of (d) pristine and (e) pruned nanobelts film. (f) On/off photocurrent response of pristine nanobelts (pink curve) and laser pruned nanobelts (green curve) to 660 nm laser. (g) On/off photocurrent response of pristine nanobelts (light blue curve) and laser pruned nanobelts (brown curve) to 808 nm laser.

CONCLUSION

In summary, we have presented an inherently efficient and high throughput approach to directly create multicolored micropatterns on CdS_xSe_{1-x} nanobelt samples. Well-defined micro structures are achievable *via* a simple focused laser beam. In addition, precise control over the fluorescence emissions of the nanobelts is another important attribute that can be achieved with this effective technique. The result is a chemical modification in the nanobelts compositions that alters the physical characteristics of the nanobelts and also provides a mechanism for patterning with multicolored domain. Moreover, followed by careful tuning of the laser power, fluorescence emissions of samples are readily controlled. As a result, a multicolored display with a reasonably wide range of controlled color at a selected location can be created on the ternary CdS_xSe_{1-x} nanobelt film. The laser modified nanobelts showed higher resistance to corrosion by acid and exhibited more superior photoconductivity. This effective approach is anticipated to be applicable to other ternary compounds as well.

METHODS

Synthesis of CdS_xSe_{1-x} Nanobelts. CdS and CdSe (Sigma Aldrich) mixed powders were used as the source precursor. A silicon wafer coated with a thin Au layer was slotted vertically inside a specially designed substrate holder. Such an arrangement promoted the growth of nanobelts with uniform stoichiometry since it is free from the influence of temperature gradient during the growth. The furnace was maintained at 650 °C for 30 min while the pressure was regulated at 1 Torr.

Characterization. Further characterizations of the pruned samples were carried out through a fluorescence microscope (FM, Olympus IX71S1F-3 Inverted Microscope), field emission scanning electron microscope (FESEM, JEOL JSM-7600F) with built-in energy-dispersive spectroscopy (EDS), photoluminescence microscope (Renishaw inVia with a Kimmon 1K Series He−Cd Laser), X-ray photoelectron spectroscopy (XPS), and X-ray diffractometer (X'PERT MPD, Cu−Kα (1.5418 Å) radiation).

Conflict of Interest: The authors declare no competing financial interest.

Supporting Information Available: Optical pictures and SEM images of CdS_xSe_{1-x} nanobelts with high uniform stoichiometry and single colors; finite element method simulation results; XRD patterns of annealed samples; photoresponse of annealed samples before and after laser pruning; reflection spectra of pristine and laser modified samples. This material is available free of charge *via* the Internet at http://pubs.acs.org.

Acknowledgment. This work is supported by the Singapore National Research Foundation under CRP Award No. NRF-CRP-4-2008-03. The authors gratefully acknowledge the financial support.

REFERENCES AND NOTES

1. Holmes, J. D.; Johnston, K. P.; Christopher Doty, R.; Korgel, B. A. Direct Control of Thickness and Orientation of Solution-Grown Silicon Nanowires. *Science* **2000**, *287*, 1471–1473.
2. Zhao, X. Y.; Wei, C. M.; Yang, L.; Chou, M. Y. Quantum Confinement and Electronic Properties of Silicon Nanowires. *Phys. Rev. Lett.* **2004**, *92*, 236805.
3. Peng, H. W.; Li, J. B. Quantum Confinement and Electronic Properties of Rutile TiO_2 Nanowires. *J. Phys. Chem. C.* **2008**, *112*, 20241–20245.
4. Beckman, S. P.; Han, J. X.; Chelikowsky, J. R. Quantum Confinement Effects in Ge [110] Nanowires. *Phys. Rev. B* **2006**, *74*, 165314.
5. Black, M. R.; Lin, Y.-M.; Cronin, S. B.; Rabin, O.; Dresselhaus, M. S. Infrared Absorption in Bismuth Nanowires Resulting from Quantum Confinement. *Phys. Rev. B* **2002**, *65*, 195417.
6. Huang, M. H.; Mao, S.; Feick, H.; Yan, H.; Wu, Y.; Kind, H.; Weber, E.; Russo, R.; Yang, P. D. Room-Temperature Ultraviolet Nanowire Nanolasers. *Science* **2001**, *292*, 1897–1899.
7. Choi, H. J.; Johnson, J. C.; He, R.; Lee, S. K.; Kim, F.; Pauzauskie, P.; Goldberger, J.; Saykally, R. J.; Yang, P. D. Self-Organized GaN Quantum Wire UV Lasers. *J. Phys. Chem. B* **2003**, *107*, 8721–8725.
8. Duan, X.; Huang, Y.; Aagrwal, R.; Liber, C. M. Single-Nanowire Electrically Driven Lasers. *Nature* **2003**, *421*, 241–245.
9. Zhong, X. H.; Feng, Y. Y.; Knoll, W.; Han, M. Y. Composition-Tunable $Zn_xCd_{1-x}Se$ Nanocrystals with High Luminescence and Stability. *J. Am. Chem. Soc.* **2003**, *125*, 8589–8594.
10. Bailey, R. E.; Nie, S. M. Composition-Tunable $Zn_xCd_{1-x}Se$ Nanocrystals with High Luminescence and Stability. *J. Am. Chem. Soc.* **2003**, *125*, 7100–7106.
11. Liang, Y. Q.; Zhai, L.; Zhao, X. S.; Xu, D. S. Band-Gap Engineering of Semiconductor Nanowires through Composition Modulation. *J. Phys. Chem. B* **2005**, *109*, 7120–7123.
12. Pan, A. L.; Yang, H.; Liu, R. B.; Yu, R. C.; Zou, B. S.; Wang, Z. L. Color-Tunable Photoluminescence of Alloyed CdS_xSe_{1-x} Nanobelts. *J. Am. Chem. Soc.* **2005**, *127*, 15692–15693.
13. Li, G. H.; Jiang, Y.; Wang, Y.; Wang, C.; Sheng, Y. P.; Jie, J. S.; Zapien, J. A.; Zhang, W. J.; Lee, S. T. Synthesis of CdS_xSe_{1-x} Nanoribbons with Uniform and Controllable Compositions *via* Sulfurization: Optical and Electronic Properties Studies. *J. Phys. Chem. C* **2009**, *113*, 17183–17188.
14. Wang, M.; Fei, G. T.; Zhang, Y. G.; Kong, M. G.; Zhang, L. D. Tunable and Predetermined Bandgap Emissions in Alloyed ZnS_xSe_{1-x} Nanowires. *Adv. Mater.* **2007**, *19*, 4491–4494.
15. Xu, H. Y.; Liang, Y.; Liu, Z.; Zhang, X. T.; Hark, S. K. Synthesis and Optical Properties of Tetrapod-like ZnSSe Alloy Nanostructures. *Adv. Mater.* **2008**, *20*, 3294–3297.
16. Chen, R. Z.; Xu, D. S.; Guo, G. L.; Gui, L. L. Preparation of Ag_2Se and $Ag_2Se_{1-x}Te_x$ Nanowires by Electrodeposition from DMSO Baths. *Electrochem. Commun.* **2003**, *5*, 579–583.
17. Liu, Y. K.; Zapien, J. A.; Shan, Y. Y.; Geng, C. Y.; Lee, C. S.; Lee., S. T. Wavelength-Controlled Lasing in $Zn_xCd_{1-x}S$ Single-Crystal Nanoribbons. *Adv. Mater.* **2005**, *17*, 1372–1377.
18. Zhai, T. Y.; Gu, Z. J.; Yang, W. S.; Zhang, X. Z.; Huang, J.; Zhao, Y. S.; Yu, D. P.; Fu, H. B.; Ma, Y.; Yao, J. N. Fabrication, Structural Characterization and Photoluminescence of Single-Crystal $Zn_xCd_{1-x}S$ Zigzag Nanowires. *Nanotechnology* **2006**, *17*, 4644.
19. Shan, C. X.; Liu, Z.; Ng, C. M.; Hark, S. K. $Zn_xCd_{1-x}Se$ Alloy Nanowires Covering the Entire Compositional Range. *Appl. Phys. Lett.* **2005**, *87*, 033108.
20. Na, C. W.; Han, D. S.; Kim, D. S.; Kang, Y. J.; Lee, J. Y.; Park, J.; Oh, D. K.; Kim, K. S.; Kim, D. Photoluminescence of $Cd_{1-x}Mn_xS$ ($x \leq 0.3$) Nanowires. *J. Phys. Chem. B* **2006**, *110*, 6699–6704.
21. Bhatacharyya, S.; Perelshtein, I.; Moshe, O.; Rich, D. H.; Gedanken, A. One-Step Solvent-Free Synthesis and Characterization of $Zn_{1-x}Mn_xSe$@C Nanorods and Nanowires. *Adv. Funct. Mater.* **2008**, *18*, 1641–1653.
22. Lu, J; Sun, C.; Zheng, M.; Mathews, N.; Liu, H.; Chen, G. S.; Zhang, X.; Mhaisalkar, S. G.; Sow, C. H. Facile One-Step

Synthesis of CdS_xSe_{1-x} Nanobelts with Uniform and Controllable Stoichiometry. *J. Phys. Chem. C* **2011**, *115*, 19538–19545.
23. Behl, M.; Seekamp, J.; Zankovych, S.; Torres, C. M. S.; Zentel, R.; Ahopelto, J. Towards Plastic Electronics: Patterning Semiconducting Polymers by Nanoimprint Lithography. *Adv. Mater.* **2002**, *14*, 588–591.
24. Pisignano, D.; Persano, L.; Raganato, M. F.; Visconti, P.; Cingolani, R.; Barbarella, G.; Favaretto, L.; Gigli, G. Room-Temperature Nanoimprint Lithography of Non-thermoplastic Organic Films. *Adv. Mater.* **2004**, *16*, 525–529.
25. Sun, Y.; Liu, Y.; Zhu, D. Advances in Organic Field-Effect Transistors. *J. Mater. Chem.* **2005**, *15*, 53–65.
26. Zhang, F.; Nyberg, T.; Inganäs, O. Conducting Polymer Nanowires and Nanodots Made with Soft Lithography. *Nano Lett.* **2002**, *2*, 1373–1377.
27. Huang, L.; Braunschweig, A. B.; Shim, W.; Qin, L.; Lim, J. K.; Hurst, S. J.; Huo, F.; Xue, C.; Jang, J.-W.; Mirkin, C. A. Matrix-Assisted Dip-Pen Nanolithography and Polymer Pen Lithography. *Small* **2010**, *6*, 1077–1081.
28. Aldred, M. P.; Contoret, A. E. A.; Farrar, S. R.; Kelly, S. M.; Mathieson, D.; O'Neill, M.; Tsoi, W. C.; Vlachos, P. A Full-Color Electroluminescent Device and Patterned Photoalignment Using Light-Emitting Liquid Crystals. *Adv. Mater.* **2005**, *17*, 1368–1372.
29. Bharathan, J.; Yang, Y. Polymer Electroluminescent Devices Processed by Inkjet Printing: I. Polymer Light-Emitting Logo. *Appl. Phys. Lett.* **1998**, *72*, 2660–2662.
30. Babentsov, V.; Riegler, J.; Schneider, J.; Ehlert, O.; Nann, T.; Fiederle, M. Deep Level Defect Luminescence in Cadmium Selenide Nano-Crystals Films. *J. Cryst. Growth* **2005**, *280*, 502–508.
31. Jing, P.; Zheng, J.; Ikezawa, M.; Liu, X.; Lv, S.; Kong, X.; Zhao, J.; Masumoto, Y. Temperature-Dependent Photoluminescence of CdSe−Core CdS/CdZnS/ZnS-Multishell Quantum Dots. *J. Phys. Chem. C* **2009**, *113*, 13545–13550.